Electronic Supplementary Material (ESI) for Journal of Materials Chemistry A.

Supplementary Information

Mechanically robust triboelectric nanogenerator with shear thickening fluid for impact monitoring

Seong-Yun Yun,[a] Il-Woong Tcho,[a] Weon-Guk Kim,[a] Do-Wan Kim,[a] Joon-Ha Son,[a] Sang-Won Lee,[a] and Yang-Kyu Choi[a]*

[a] School of Electrical Engineering, Korea Advanced Institute of Science and Technology (KAIST), 291 Daehak-ro, Yuseong-gu, Daejeon 34141, Republic of Korea

* Address correspondence to ykchoi@ee.kaist.ac.kr

1. 3D-printed molds for manufacturing of STF-TENG and used objects for evaluation of both impact-absorbing property and mechanical robustness of STF-TENG

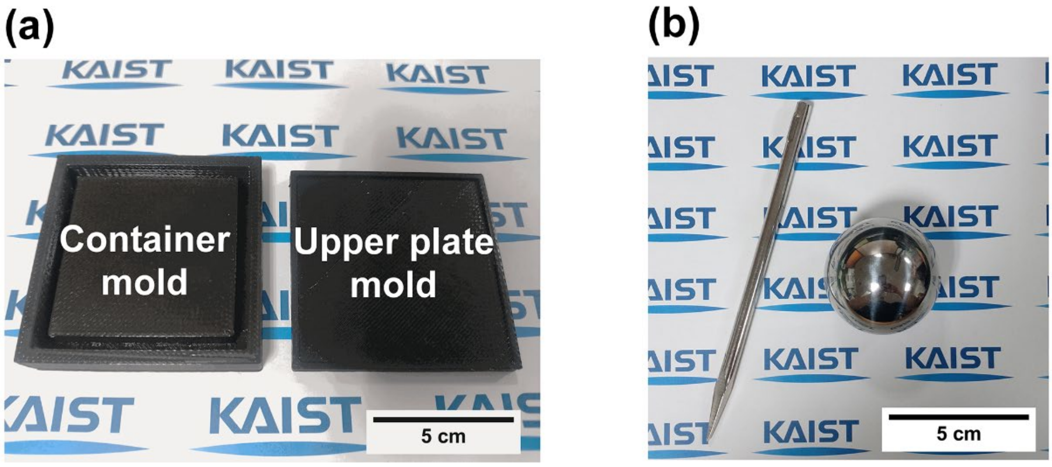

Figure S1. (a) Optical photograph of the 3D-printed molds for manufacturing of STF-TENG. Left image is the 3D-printed mold for manufacturing a container. Right image is 3D-printed mold for manufacturing an upper plate served as a lid. (b) Optical photograph of the metal ball for evaluation of impact-absorbing property and the pointed gimlet for assessment of mechanical robustness. All scale bars are 5 cm.

2. Resistance measurement of the STF

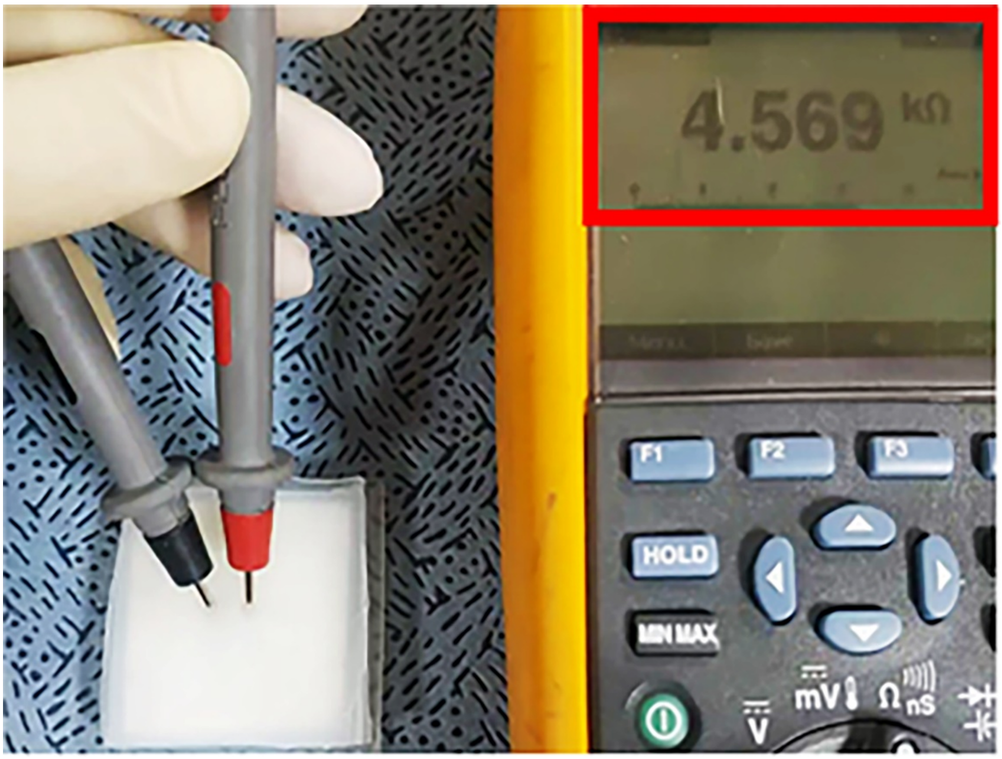

Figure S2. Resistance of the shear thickening fluid.

3. Particle size distribution of corn starch and SEM image of NaCl

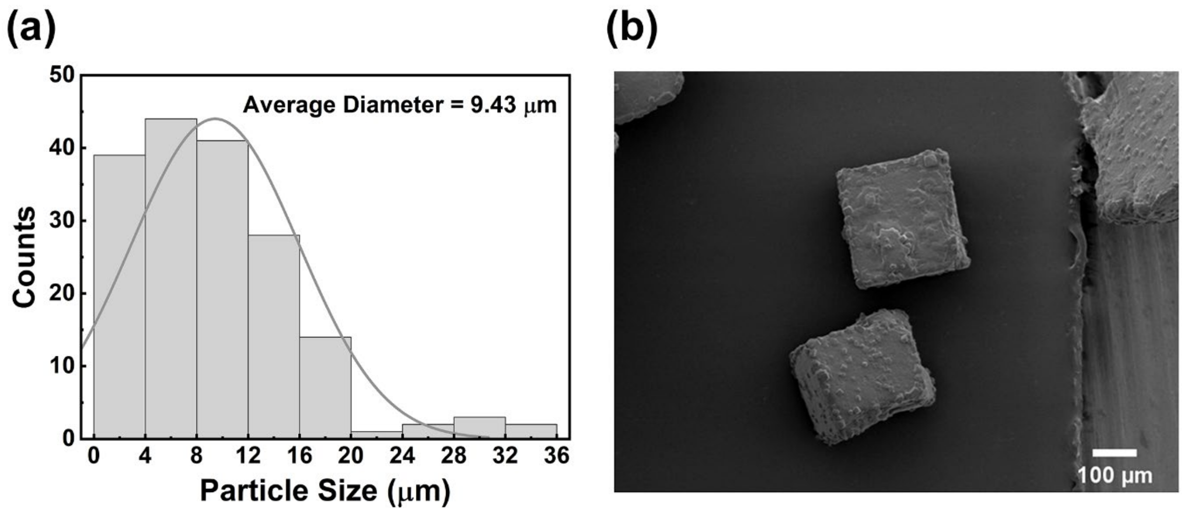

Figure S3. (a) Particle size distribution of the corn starch. (b) SEM image of NaCl. A scale bar is 100 μm.

4. Experimental setup for measurement of electrical output performance and contact force

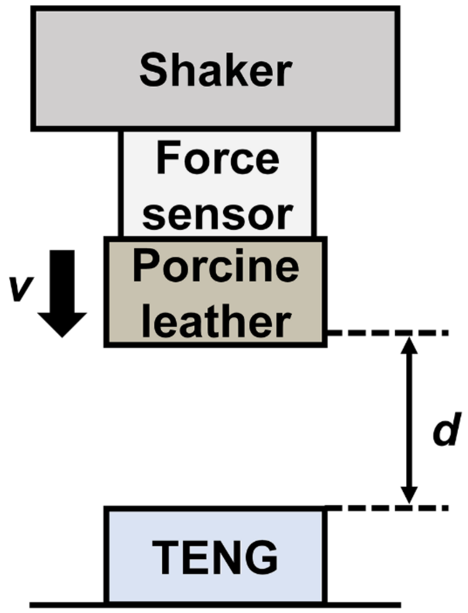

Figure S4. Experimental setup for the measurement of the electrical output performance and the contact force of the S-TENG, the L-TENG, and the STF-TENG.

5. Comparison of transferred charge density among S-TENG, L-TENG, and STF-TENG

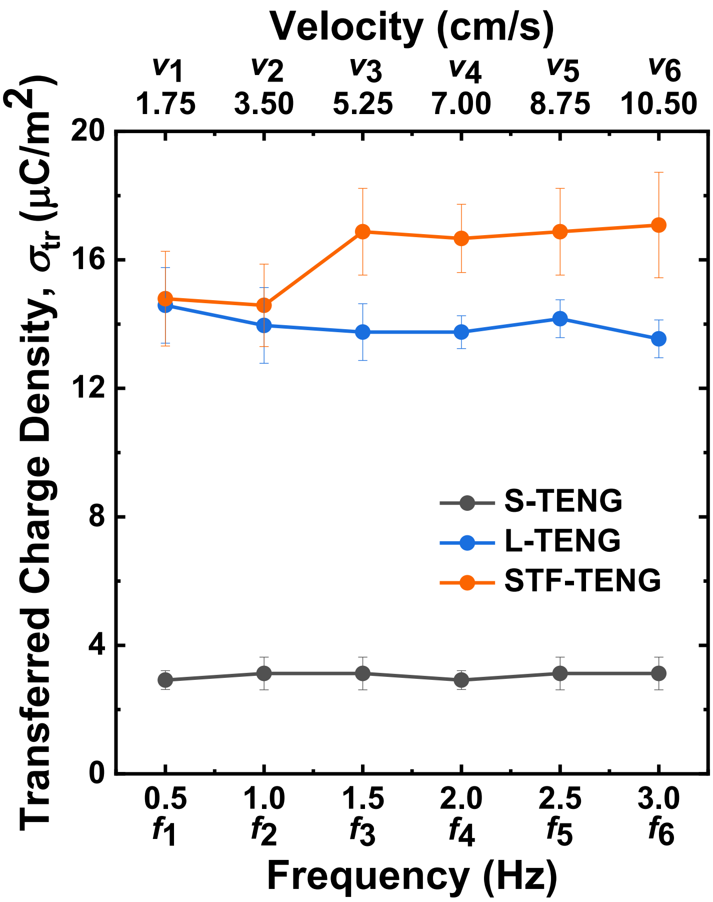

Figure S5. Comparison of transferred charge density (σ_{tr}) among the S-TENG, the L-TENG, and the STF-TENG for various contact velocities.

6. Electrical output performances of S-TENG, L-TENG, and STF-TENG

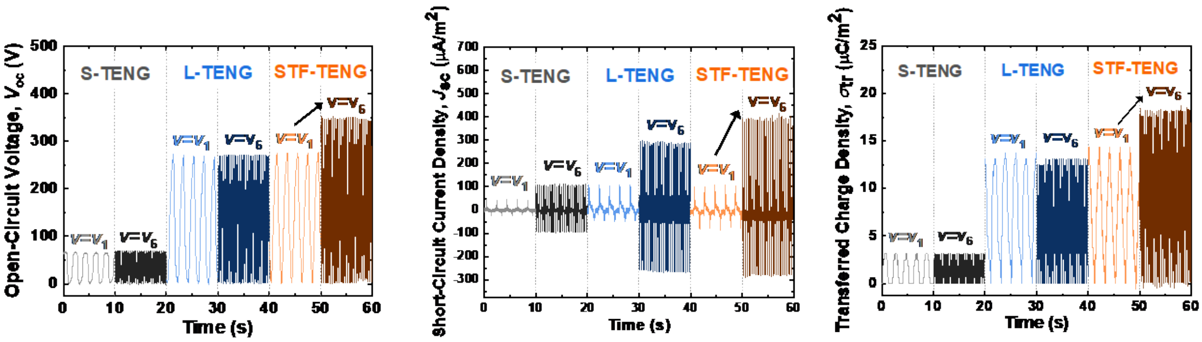

Figure S6. Waveforms of three electrical output performances for S-TENG, L-TENG, and STF-TENG at v_1 and v_6 (a) V_{oc}, (b) J_{sc}, (c) σ_{tr}.

7. Measured impact force on flat surface

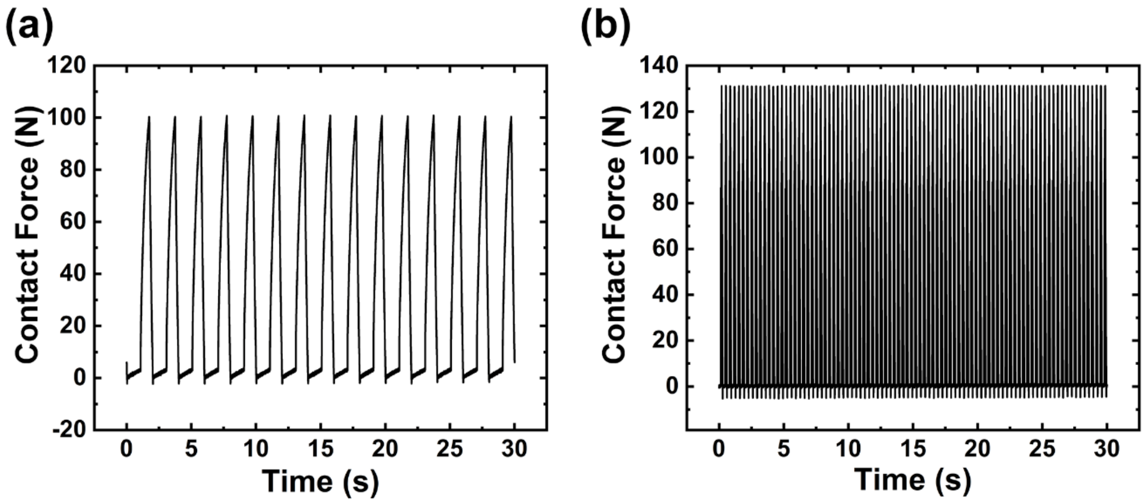

Figure S7. Measured impact force (contact force) on flat surface. (a) Contact force at v_1. (b) Contact force at v_6.

8. Comparison of peak power density among S-TENG, L-TENG, and STF-TENG

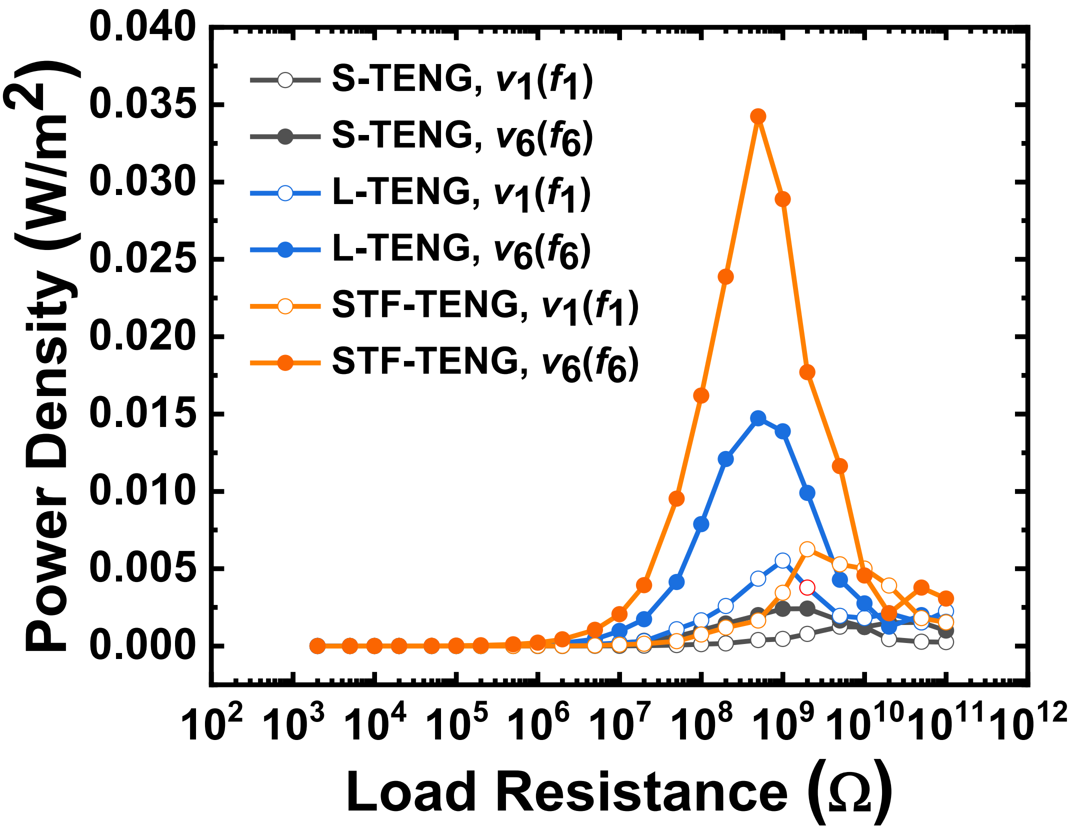

Figure S8. Comparison of extracted peak power density from the S-TENG, the L-TENG, and the STF-TENG at v_1 and v_6.

9. Demonstration of STF-TENG as a power source to drive LEDs

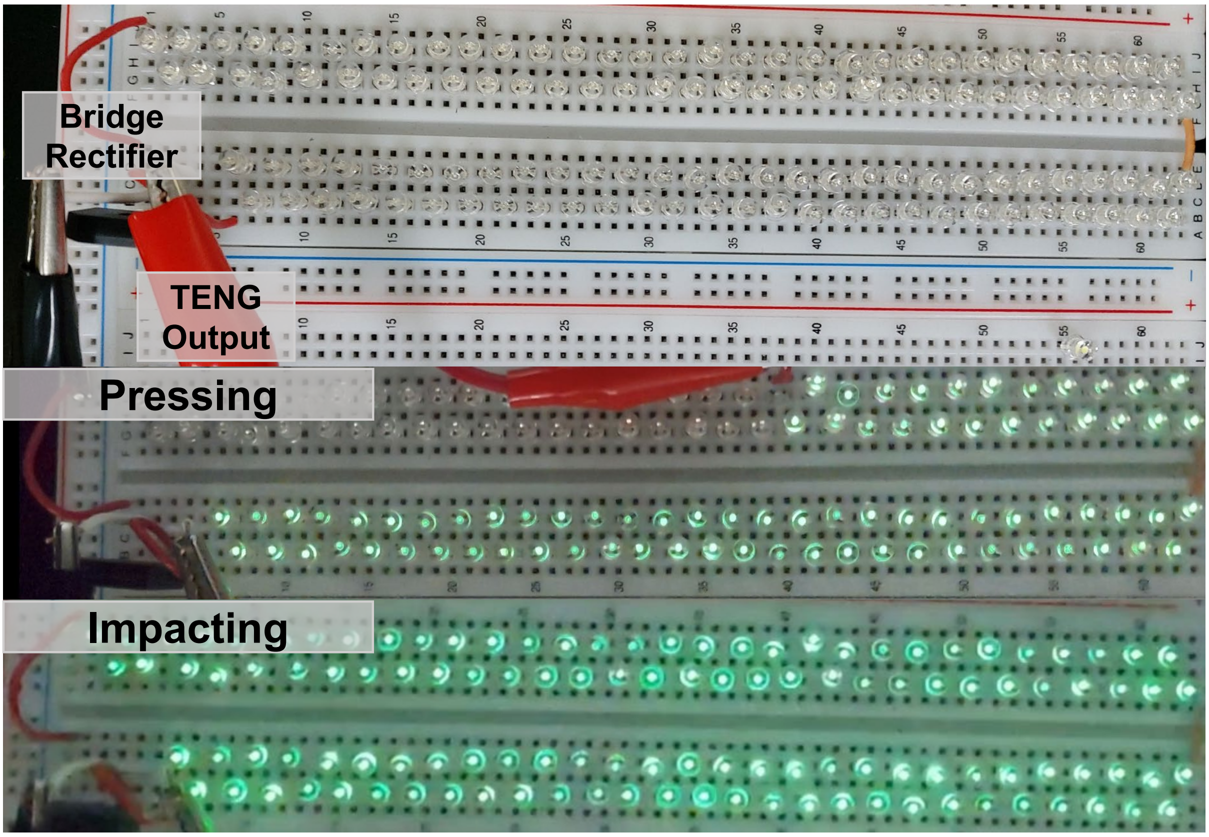

Figure S9. Optical photographs to light up LEDs by power generated from the STF-TENG. Whereas 80 LEDs were turned on by pressing, 119 LEDs were turned on by impacting.

10. Experimental setup for measurement of impact force

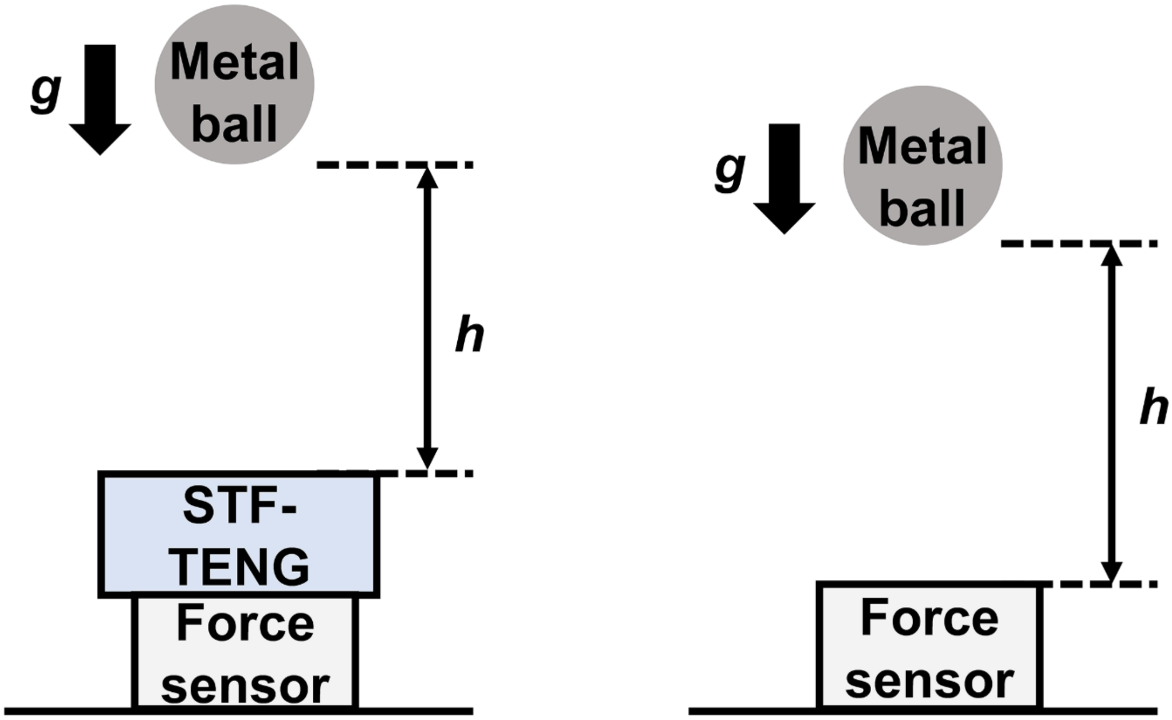

Figure S10. Experimental setup for measurement of impact force by a free-falling metal ball with a height of *h* above the STF-TENG (left) and above the force sensor (right), respectively.

11. Characterization of impact-absorbing property

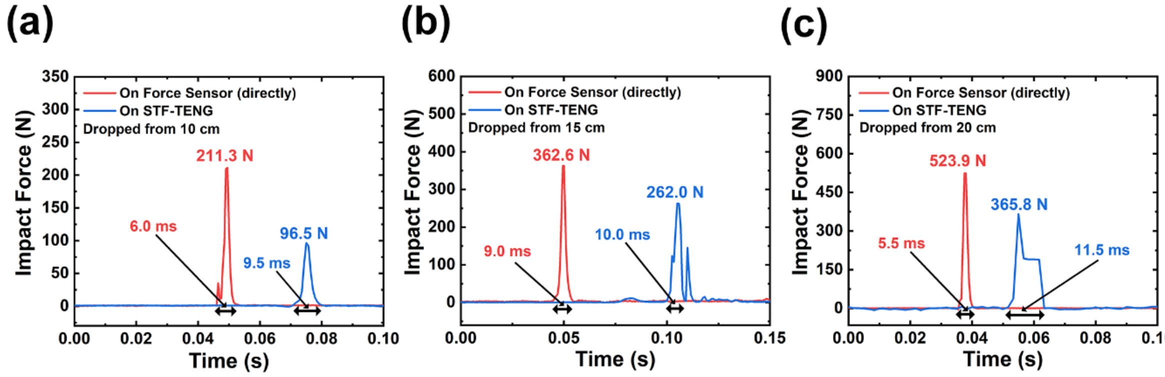

Figure S11. Comparison of impact forces between on the STF-TENG and directly on the force sensor for various *h*. (a) Compared impact forces at *h*=10cm. (b) Compared impact forces at *h*=15 cm. (c) Compared impact forces at *h*=20 cm.

12. Output current density generated by dropping metal ball

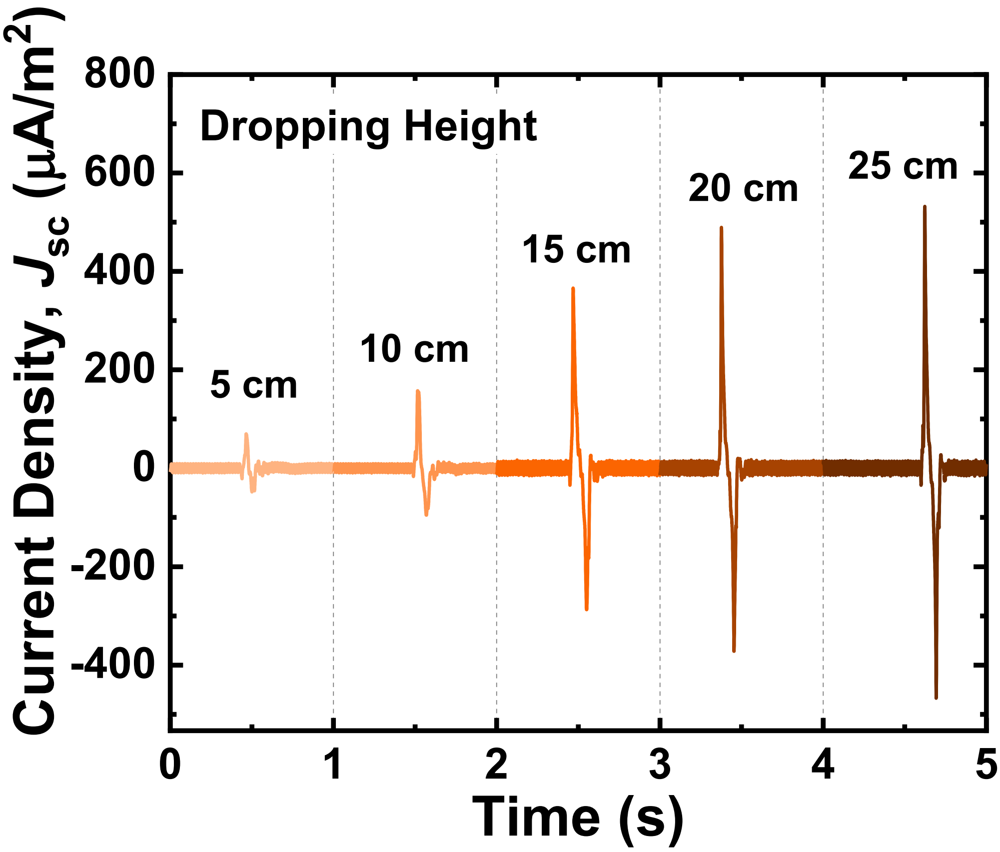

Figure S12. Increased output current density with the increased dropping height (*h*) of the metal ball.

13. The impact force applied to the STF-TENGs with various STF thicknesses

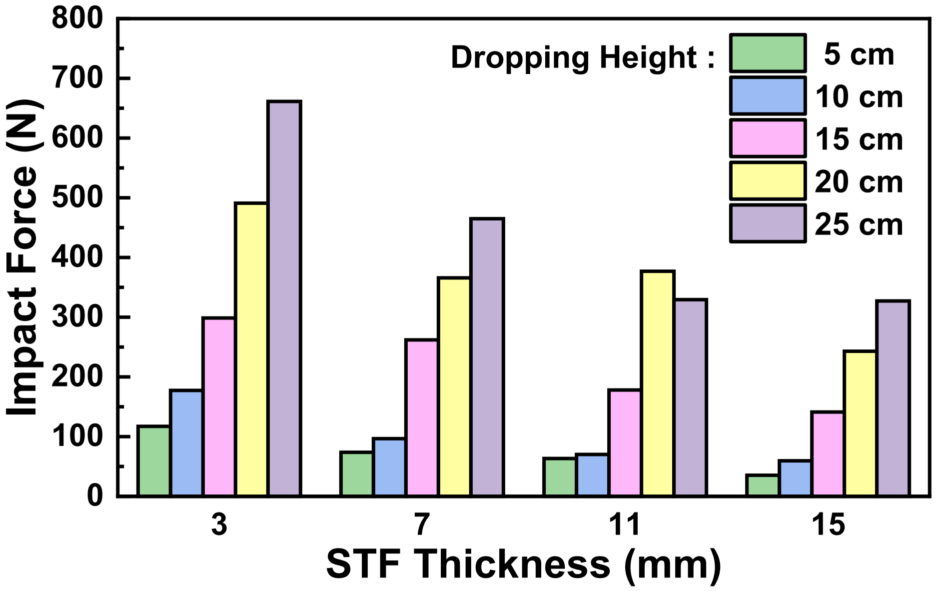

Figure S13. Comparison of impact force for various STF thicknesses.

14. Poor mechanical robustness of L-TENG by stabbing

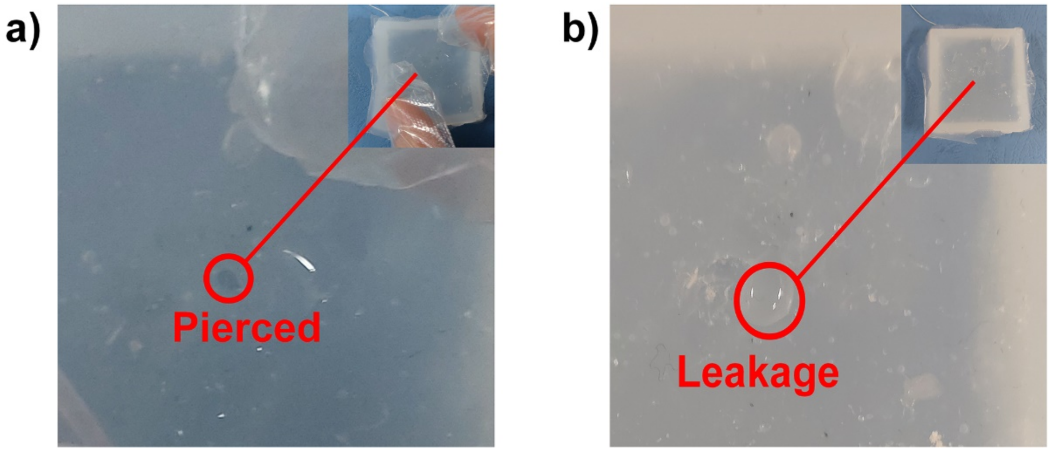

Figure S14. Optical photographs of destroyed L-TENG. (a) Pierced outer silicone rubber shell. (b) Water bead formed by leakage *via* the pin hole after 10 times of the stabbing with the pointed gimlet.

15. Output current density for 8-types of motion

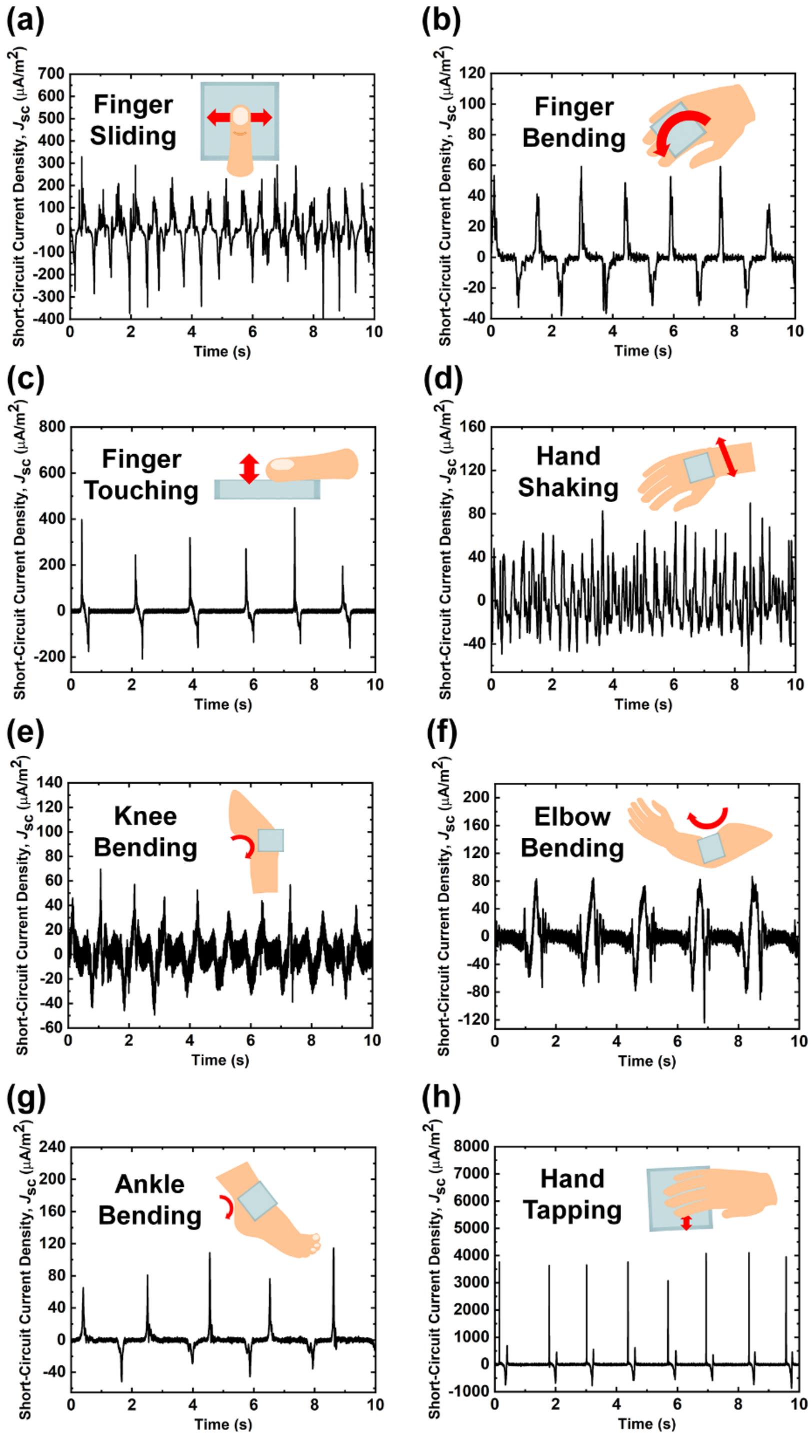

Figure S15. Output current density for 8 types of human body motion. (a) J_{sc} with finger sliding. (b) J_{sc} with finger bending. (c) J_{sc} with finger touching. (d) J_{sc} with hand shaking. (e) J_{sc} with knee bending. (f) J_{sc} with elbow bending. (g) J_{sc} with ankle bending. (h) J_{sc} with hand tapping.

Table S1. Different filler materials embedded in S-TENG, L-TENG, and STF-TENG

	Recipe	Schematic
S-TENG	CB (9.0 wt %) + Ecoflex	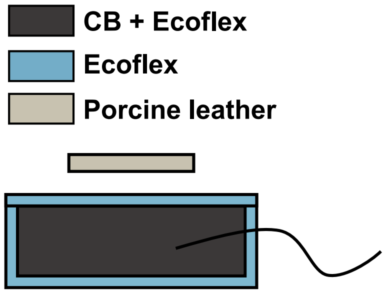
L-TENG	NaCl (0.36 g/mL) + Water	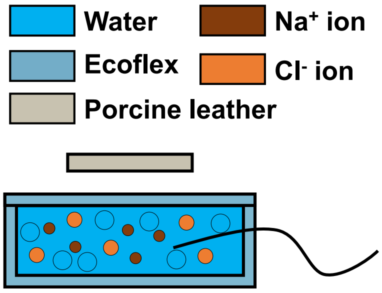
STF-TENG	NaCl (0.36 g/mL) + Water : Starch (45 : 55)	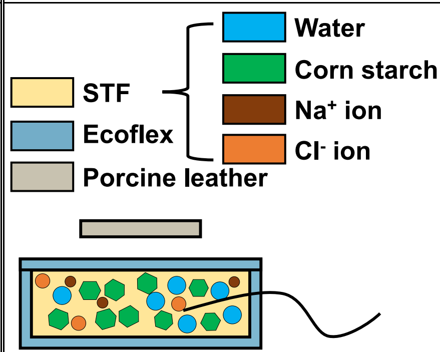

Supplementary Note 1. A detailed description of comparing the operations of the S-TENG, the L-TENG, the STF-TENG

As shown in Figure S15, it is assumed that the waveforms of the normalized impact force are the same for fair comparison among the S-TENG, the L-TENG, and the STF-TENG. Additionally, it is also assumed that force at time t_3 corresponds to critical shear rate of the STF. The schematic of different behavior for the S-TENG, the L-TENG, and the STF-TENG are shown in Table S2. For better understanding, all the schematics are exaggerated along with a vertical direction.

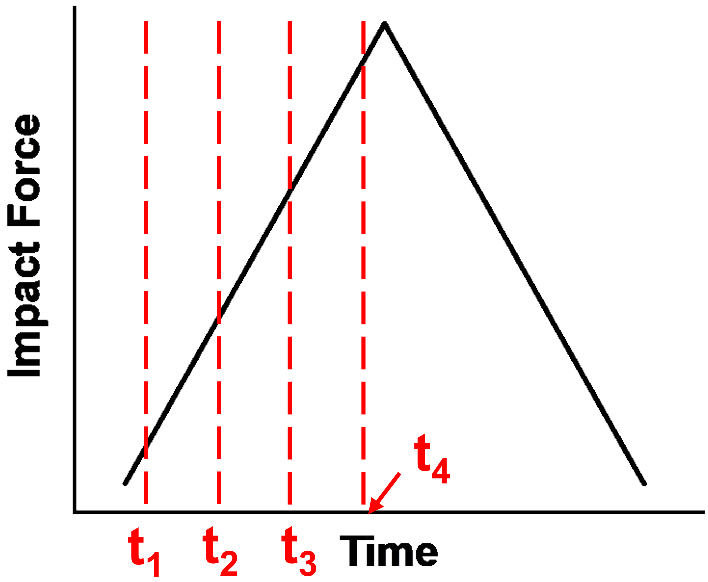

Figure S16. Normalized contact force waveform, which is assumed to be the same for the S-TENG, the L-TENG, the STF-TENG

At t_1:

The porcine leather just touches the silicone rubber for all TENGs. There is no difference.

At t_2:

Because the solid is relatively hard, the deformation is scarcely occurred in the S-TENG. On the other hand, for both the L-TENG and the STF-TENG, deformation of the flexible silicone rubber results in increasing an effective contact area. The porcine leather snuggles into the deformable silicone rubber by virtue of fluidity.

At t_3:

The deformation does not occur in the S-TENG so that the porcine leather does not move downward. For the L-TENG, increased contact force is measured when the porcine leather is moved deeply and downwardly. For the STF-TENG, the STF is hardened at the critical shear rate. Nevertheless, the porcine leather tended to be moving deeply and downwardly until the critical shear rate is reached.

At t_4:

The deformation is not occurred in the S-TENG, however, the further deformation is still occurred in the L-TENG. For the STF-TENG, the porcine leather does not move further downwardly owing to the hardened STF.

Table S2. Schematic of the S-TENG, the L-TENG, the STF-TENG at t_1, t_2, t_3, and t_4

	$t = t_1$	$t = t_2$	$t = t_3$	$t = t_4$
S-TENG				
L-TENG		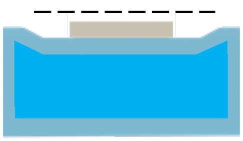	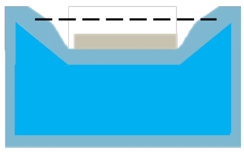	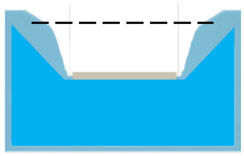
STF-TENG		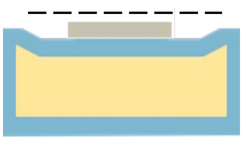	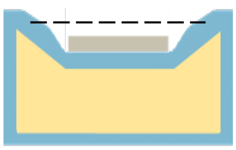	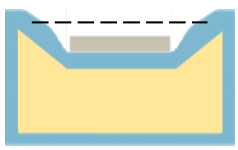

Porcine leather | Ecoflex | CB + Ecoflex | Water | STF